PHOTONICS Research

# Observation of controllable tightly and loosely bound solitons with an all-fiber saturable absorber

Tianyu Zhu,[1] Zhaokun Wang,[1,2] D. N. Wang,[1,*] Fan Yang,[1] and Liujiang Li[1]

[1]College of Optical and Electronic Technology, China Jiliang University, Hangzhou 310018, China
[2]e-mail: 16a0402091@cjlu.edu.cn
*Corresponding author: dnwang@cjlu.edu.cn

Received 11 October 2018; revised 15 November 2018; accepted 19 November 2018; posted 20 November 2018 (Doc. ID 348021); published 17 December 2018

**A hybrid no-core fiber (NCF)–graded index multimode fiber (GIMF) structure is used as a saturable absorber (SA) for mode-locked laser operation. Such an SA supports various types of soliton outputs. By changing the cavity parameters, not only the spatiotemporal mode-locking states with a stable single pulse but also tightly and loosely bound solitons are generated. Single 35.5 pJ solitons centered at 1568.5 nm have a 4 nm spectral full-width at half-maximum and an 818 fs temporal duration. Tightly bound soliton pairs with continuously tunable wavelength from 1567.48 nm to 1576.20 nm, featured with an ~700 fs pulse train with a separation of 2.07 ps, have been observed by stretching the NCF-GIMF structured device. Meanwhile, several different pulse separations from 37.57 ps to 56.46 ps of loosely bound solitons have also been realized. The results provide help in understanding the nonlinear dynamics in fiber lasers.** 

https://doi.org/10.1364/PRJ.7.000061

## 1. INTRODUCTION

A bound soliton, also known as a soliton molecule or bound state, is a fascinating phenomenon of soliton dynamics, while multiple solitons are energy quantized and bounded together due to the peak-power limiting effect of the laser cavity [1] and the balance of repulsive and attractive forces between solitons caused by nonlinear and dispersive effects [2]. The bound soliton shows characteristics of a strong phase-locking phenomenon between soliton pulses and the nearly fixed pulse separation. Bound solitons with organized structures provide a simple and direct method of extending the coding alphabet to enlarge the data-carrying capacity of optical fiber [3]. As a result, much attention has focused on the phenomenon of bound solitons, as they may help in solving the upcoming Internet traffic jam in optical communication systems.

The bound soliton was theoretically proposed based on the model of the nonlinear Schrödinger equation and complex Ginzburg–Landau equation in fiber lasers in the 1990s [4–6]. The phenomenon of bound solitons was first experimentally reported in 2001 with the rise of optical fiber communication applications [7]. With the gradual progress in novel saturable absorbers (SAs) and new measuring equipment, the experimental parameters can be precisely controlled to realize various types of bound solitons in fiber lasers [8]. Up to now, with the alteration of cavity parameters, different bound solitons including soliton pairs, soliton triplets, soliton quartets, etc., have been successively generated in mode-locked fiber lasers [9]. Among them, the most common one in fiber lasers is the bound soliton pair. It is a stable two-soliton bound state with the same pulse width and intensity due to the balance of forces by dissipation nature of fiber lasers [10–14]. The soliton bound pairs can be classified into tightly and loosely bound soliton pairs according to the different temporal separation of the two pulses. For tightly bound soliton pairs, the time separation and the corresponding spectrum modulation period are fixed tightly and steadily. For loosely bound soliton pairs, the soliton separation is found to be relatively not tight, and the spectrum modulation period is also unstable.

It has been found that the laser gain medium with high gain coefficient and short length is more favorable for the generation of bound solitons at the fundamental repetition rate [15]. Moreover, the parameters of SA can directly and significantly influence the formation of the stable and controllable bound states. So far, a number of SAs have been reported for the generation of soliton pairs in mode-locked fiber lasers, including polarization additive pulse mode locking (P-APM) [16], nonlinear polarization evolution (NPE) [17], single-wall carbon nanotubes (CNTs) [18], semiconductor SA mirrors (SESAMs) [19], graphene [20], topological insulators (e.g., $Bi_2Se_3$ [21]), molybdenum disulphide ($MoS_2$ [22]), and black phosphorus (BP) [23]. Recently, Wang *et al.* [24,25] proposed a new type of all-fiber SA based on the nonlinear multimode interference

effect in graded index multimode fiber (GIMF). A light intensity-dependent transmission can be obtained due to the core diameter mismatch between the GIMF and the single-mode fiber (SMF). Compared with material-based SAs, such as the two-dimensional (2D) nanomaterial represented by graphene [20–23,26], our artificial structure SAs have many advantages, such as versatility and simplicity, ease of implementation, being independent of laser operation wavelength, the high damage threshold of supporting high-power operation, and especially the capability of tunable wavelength and controllable modulation depth when being stretched. The GIMF provides an abundance of novel and complex nonlinear phenomena when ultrashort pulses are generated. Thus, the GIMF-based SA provides an efficient approach for the evolution of bound solitons.

In this paper, based on a net-anomalous-dispersion mode-locked laser using an all-fiber SA, both stable tightly and loosely bound soliton pairs with a fixed phase difference of $\pi$ are realized for the first time, to our knowledge. The no-core fiber (NCF)-GIMF SA with flexible controllable peak wavelengths and modulation depths makes great contributions to the generation of different types of bound solitons. The tunable central wavelength operation from 1567.48 nm to 1576.20 nm in tightly bound states is achieved by adjusting the stretching length of the NCF-GIMF device. The loosely bound states with gradually increased pulse separation from 37.57 ps to 56.46 ps are also obtained by slightly stretching the SA, corresponding to the decrease of spectral modulation period and amplitude. These two tunable phenomena may be helpful for the application of bound states in the field of high-capacity soliton fiber communication systems. In addition, we observe some abnormal states of bound soliton pairs that contain complex and stable modulation periods in spectra for the first time.

## 2. PRINCIPLES OF BOUND SOLITONS

It is known that the fiber laser is a complex intracavity dissipative system with a composite balance of nonlinearity, dispersion, gain, and loss [27]. As the balance can withstand only finite nonlinear phase shifts, the high-pumping light makes the single pulse split into several pulses of lower peak energy. These pulses interact with each other through repulsive and attractive forces [8]. The attractive force is provided by phase modulation, and the repulsive force is powered by soliton interaction. Due to the interaction of these two forces, some special stable soliton states appear, including harmonic mode locking, pulse bunching, and bound solitons. Among them, bound solitons are the most unusual states where certain individual pulses are bounded together and keep constant time separations and fixed phase differences, besides holding the same spectral and temporal profiles.

There are three types [10] of strong soliton interactions: direct, long-range, and global soliton interactions. The direct soliton interaction happens when they are closely spaced. It contains attractive and repulsive interaction, depending on the phase difference between the adjacent solitons, and decreases as the soliton separation increases. When the time separation between solitons exceeds tens of times the time bandwidth of the soliton itself, the direct soliton interaction can be ignored. The long-range soliton interaction happens when the resonant dispersive waves start operating. Note that the long-range interaction is not affected by the phase difference. The global type of soliton interaction comes from the unstable continuous wave in the cavity. To conclude, three types of soliton interactions have different interaction ranges and strength operation conditions, and they can coexist or exist alone. By adjusting various parameters of the fiber laser, the balance of three kinds of forces can be established. Then the bound states of multiple solitons can be established as well, and maintain a fixed phase relationship and pulse separation. Whenever the equilibrium is established, there will be a bound state with a certain phase difference and pulse separation. In practice, the balance may be broken due to the disturbance of the unavoidable environmental parameters. However, when the equilibrium is re-established, there are different types of bound states.

The double soliton bound states are the most common in the bound states of multiple solitons. In general, according to the phase difference of the two solitons, the soliton bound pairs can be divided into four types, including 0, $-\pi/2$, $+\pi/2$, and $\pi$. In the literature, soliton pairs with 0 phase difference are called in-phase soliton pairs, while those with $\pi$ are called out-of-phase soliton pairs. The common feature of the in-phase and out-of-phase soliton pairs is the same axisymmetric spectrum. The spectral center of the in-phase soliton pairs is the minimum, whereas that of the out-of-phase soliton pairs is the maximum. The common characteristic of the $-\pi/2$ and the $+\pi/2$ phase-difference soliton pairs is that the center of the spectrum is the minimum, while the two peaks are in the middle of the spectrum. The $-\pi/2$ phase-difference soliton pairs have a feature that the right peak is larger than the left peak in their spectrum. By comparison, the $+\pi/2$ phase-difference soliton pairs have a feature that the left peak is larger than the right peak. Thus, the phase difference can be easily calculated and identified from the spectra and the separation of the pulses.

It has been proved that modulation periods depend on the time separations of the pulses. Such pulse separations increase as the phase difference increases. The phase difference is proportional to the pump power and the cavity length. A higher pump power leads to a higher peak pulse power and a longer cavity length and can accumulate a stronger nonlinear effect. Both the excessive power and the nonlinear effect [22] lead to the appearance and aggravation of the pulse-splitting phenomenon. There are usually two ways to produce pulse splitting when keeping the pump power constant and the cavity length fixed [28]. One is to increase the saturable peak power or decrease the modulation depth of the SA and the other is to increase pulse duration by increasing cavity dispersion. Our tuning method belongs to the former one. By stretching the SA structure of the NCF-GIMF, a smaller modulation depth of SA leads to a wider pulse separation [20], which then leads to a smaller spectral modulation period and lower modulation amplitude.

## 3. EXPERIMENTAL RESULTS

### A. Experimental Setup

In order to intensively study the propagation characteristics of the solitons, an all-fiber laser system based on an NCF-GIMF SA

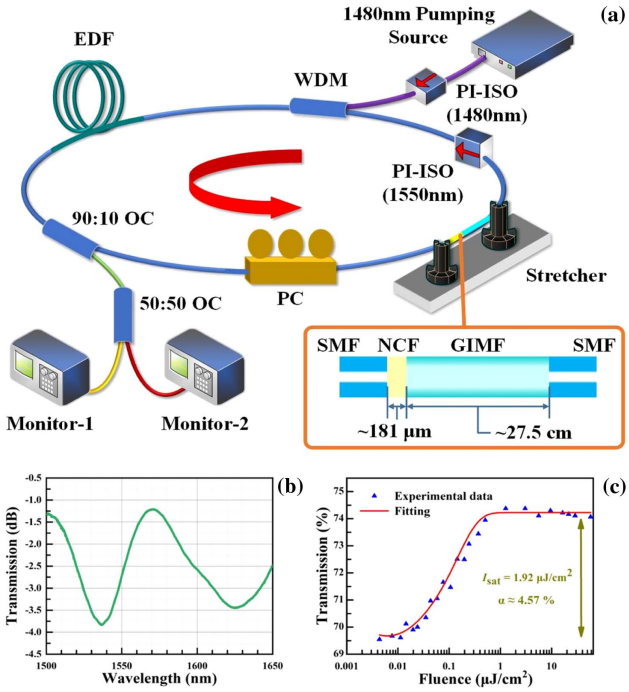


**Fig. 1.** (a) Schematic diagram of the experimental setup. Red arrow represents the direction of laser transmission, and the small diagram shows the SA structure; (b) transmission spectrum of the NCF-GIMF device; (c) nonlinear saturable absorption curve of the NCF-GIMF device.

in the negative dispersion regime is fabricated. As shown in Fig. 1(a), the 1480 nm forward-pumping light enters the fiber ring cavity via a wavelength division multiplexer (WDM). The 1480 nm polarization-independent isolator PI-ISO (1480 nm) is installed to protect the pumping source. The ring cavity consists of a WDM, a section of erbium-doped fiber (EDF), a 90:10 optical coupler (OC) with 10% output, a polarization controller (PC), the NCF-GIMF device attached to a stretcher with a precision of larger than 10 μm, and a 1550 nm PI-ISO. The total length of the ring cavity is ~13 m, including an SMF of ~10 m and a section of EDF of ~3 m, with overall net anomalous dispersion. The PI-ISO (1550 nm) is used to ensure the unidirectional operation of the ring cavity. The PC is included to finely adjust the birefringence and optimize the mode-locking operation. The output pulses can be simultaneously analyzed via a 50:50 OC by an optical spectrum analyzer (OSA) (Yokogawa, AQ6370D) with 0.02 nm resolution, a 1 GHz digital photodetector oscilloscope (Tektronix, TDS5104B), a 9 kHz–3.2 GHz radio frequency (RF) spectrum analyzer (Siglent, SSA3032X), a 5 GHz photodetector (Thorlabs, DET08CFC/M), and a second-harmonic autocorrelator (APE, PulseCheck 150).

The SA is fabricated by sequentially fusing splicing of an SMF, an NCF of ~181 μm, a GIMF of ~27.5 cm, and an SMF, as shown in the inset in Fig. 1(a). The lengths of SIMF and GIMF are not intentionally chosen. The biggest advantage of the NCF-GIMF device is that there is no need to control the lengths of the NCF and GIMF. The SA effect of the NCF-GIMF results from the nonlinear multimode interference effect (NL-MMI). The introduction of NCF is used to expand the light and increase the mode field diameter at the entrance of the GIMF, which can improve the performances of switching and intensity discrimination, benefiting from the suppression of power leakage into the radiation and cladding modes. Compared with the SIMF [24], the NCF with larger NA and equivalent core diameter has superiority for expanding the mode diameter. Also, the introduction of NCF removes the strict limit on the length of GIMF, making the SA device feasible in the experiment and providing a more flexible means of making an SA based on NL-MMI. Hence, there is essentially no limit on the length of GIMF. The transmission spectrum of the NCF-GIMF device in a spectral range from 1430 nm to 1630 nm is measured by use of an OSA and a broadband light source (BBS Amonics), as shown in Fig. 1(a). The device shows a relatively flat absorption curve with the loss of less than 2.5 dB within the measurement range. The nonlinear saturable absorption curve at different stretching lengths is shown in Fig. 1(b). It can be seen in Fig. 1(c) that the device exhibits typical characteristics of saturable absorption, in which the transmission increases with the rise of pulse fluence. The modulation depth, saturation intensity, and nonlinear loss of the SA are measured as 4.57%, 1.92 μJ/cm$^2$, and ~69.71%, respectively. Obviously, such an SA can be used in the fiber laser for producing stable mode-locked pulse trains.

### B. Conventional Solitons

First, the conventional solitons are generated at the pump power of 70 mW by appropriately adjusting the PC, and the corresponding output results are displayed in Fig. 2. The clearly Kelly spectral sidebands can be observed in Fig. 2(a), which certifies its anomalous dispersion cavity. The center wavelength is fixed at 1568.4 nm with a 3 dB bandwidth of ~4 nm. Note that the basement optical spectrum is asymmetric, which results from the oscillating at the edge of the gain range. As shown in Fig. 2(b), assuming a sech$^2$ pulse profile, the autocorrelation trace indicates a pulse width of ~818 fs within a 4 ps range. Thus, the time-bandwidth product (TBP) is calculated to be ~0.338, which is slightly larger than that of a standard transform-limited pulse, indicating a small chirp of the pulses. In Figs. 2(c) and 2(d), the oscilloscope pulse train and radio frequency (RF) spectrum are provided, respectively. The pulse period is ~60.09 ns in accordance with the repetition rate of ~16.64 MHz, which demonstrates that the pulse operates at the fundamental frequency state. From Fig. 2(d), the first RF peak is located at 16.64 MHz and the signal-to-noise ratio (SNR) with 10 Hz resolution bandwidth (RBW) and 500 kHz span is up to ~74 dB, which indicates the high stability of operation. The maximum average output power at the fundamental frequency is measured to be ~591.5 μW, corresponding to the single pulse energy of ~35.55 pJ. Being superior to the other SA materials, the $SiO_2$ of MMI can support the higher threshold of optical-power-induced thermal damage at room temperature and contribute to long-term reliability of the mode-locked fiber laser. To evaluate the stability, the system is tested over 24 h, and the mode-locked operation is stable in the output spectrum, pulse width, output power, and repetition rate.

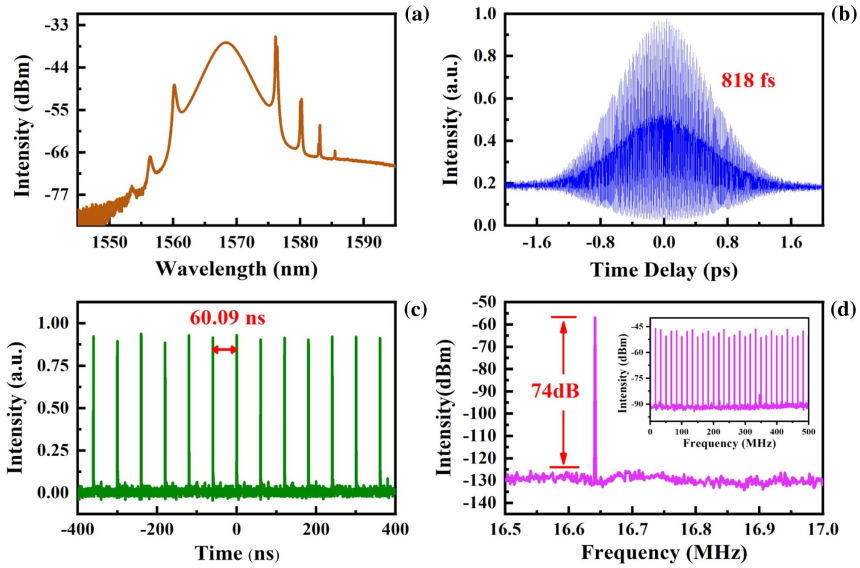


**Fig. 2.** Conventional mode-locked single soliton outputs. (a) Optical spectrum; (b) autocorrelation trace; (c) pulse train; (d) RF spectrum.

### C. Tightly Bound Solitons with Tunable Wavelengths

In the anomalous dispersion regime, the natural balance between the nonlinear effect and dispersion can contribute to formation of an optical soliton. However, when the intra-cavity pulse energy exceeds the threshold value, excessive nonlinearity will result in the breakup phenomenon of the solitons, which further leads to the appearance of an additional soliton pulse [25].

Taking the importance of a fixed-phase relationship for forming bound states into consideration, we carefully adjust the PC under the same pump power of 70 mW. The single soliton finally splits into two pulses and then evolves into the stable tightly bound soliton pairs. The average output power drops to 390 μW instantaneously due to pulse splitting. It can be clearly seen in Fig. 3(a) that the spectrum exhibits a regular and evident modulation of high contrast accompanied by the Kelly sidebands, which results from the interference fringes of the two closely spaced solitons. The spectral modulation has a symmetric structure with a central dip at the wavelength of 1573.72 nm and a spatial period of ~3.78 nm. The corresponding autocorrelation trace is illustrated in Fig. 3(b). There are three peaks exhibiting the same pulse duration of 662 fs, fitted by a $\text{sech}^2$ profile. It also shows a constant pulse time separation of ~2.07 ps, which matches the spectral modulation period (calculated from the Fourier transform). The height ratio of 1:2:1 and the same width of the three peaks in Fig. 3(b) indicate that the two bound solitons have identical intensity, pulse duration, and a constant separation. Here, the inter-pulse separation is calculated to be ~3.13 times

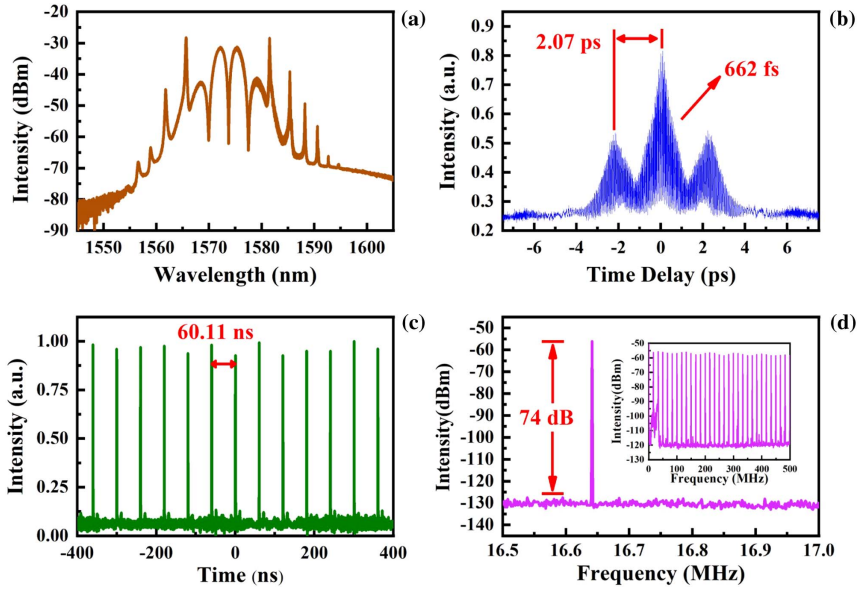


**Fig. 3.** Output of stable tight soliton pairs. (a) Optical spectrum; (b) autocorrelation trace; (c) pulse train; (d) RF spectrum.

the pulse width, demonstrating that the solitons in the bound state are strongly interacting with each other. The optical spectrum shown in Fig. 3(a) combined with the optical autocorrelation trace in Fig. 3(b) proves that the phase difference between the two mode-locked solitons is around $\pi$, and the bound state is tightly bound soliton pairs. Such tightly bound solitons are impossible to be exhibited by our oscilloscope due to the bandwidth limitation of the oscilloscope and the photodetector. Both Figs. 3(c) and 3(d) illustrate the corresponding pulse train and RF spectrum. The 16.63 MHz repetition rate of the output pulse train and over 74 dB SNR at the fundamental frequency state confirm the high mode-locking stability and low pulse energy fluctuation of our fiber laser. In addition, the long-term stability of tightly bound soliton pairs has also been assessed over several hours without any introduced perturbation.

The MMI self-imaging phenomenon enables the SMF-GIMF-SMF structure as an all-fiber bandpass filter, which can provide essential wavelength selection in ultra-short-pulse fiber lasers [29,30]. Considering the transmission peak is inversely proportional to the length of GIMF, the bandpass wavelength of the filter can be tuned by changing the GIMF length. In the state of tightly bound pairs, there is a strong phase-locking phenomenon between the two soliton pulses, and the time separation is nearly fixed, which leads to a steady spatial modulation period. Thus, its existence is robust and not easily affected by external disturbances within a certain range. It is called a super-soliton [31], which can be treated as an independent unit to form other soliton states, including stretching, compressing, and tuning.

We successfully realize the wavelength tunable operation in the state of tightly bound soliton pairs. By stretching the NCF-GIMF device from 0 μm to ~40 μm, the wavelength of the central dip is tuned in a range of 8.72 nm from 1567.48 nm to 1576.20 nm. During the tuning process, only the length of the NCF-GIMF device is adjusted, and a mechanical displacement platform is used to accurately control the stretching length of the SA for each tuning operation. By changing the stretching length, the wavelength can be switched back and forth, while the modulation periods of the spectra remain close to ~3.7 nm. Figure 4 gives the summary of the spectra with central wavelengths of 1567.48 nm, 1573.60 nm, 1573.72 nm, 1574.64 nm, 1575.79 nm, and 1576.20 nm, respectively, and it can be clearly seen that the spectra maintain the fixed-phase difference of $\pi$. The corresponding autocorrelation trace shows no significant variation compared with that shown in Fig. 3(b), and the tightly bound soliton pairs at different wavelengths have similar characteristics. Thus, continuous wavelength tunability of the bound soliton fiber laser is experimentally obtained through exploiting an NCF-GIMF device both as the SA and the intra-cavity filter simultaneously. It should also be noted that the influence of continuous light in the cavity on the Kelly sideband results in slight distortion of the spectral profile during the tuning process.

The variation of the corresponding central wavelength shifts of the central dip with the stretching length of the NCF-GIMF device is also shown in Fig. 5, where it can be found that there is a linear positive correlation between the stretching length of the SA and the central wavelength of tightly bound soliton pairs. The linear fitting coefficient $R^2$ is up to ~0.98.

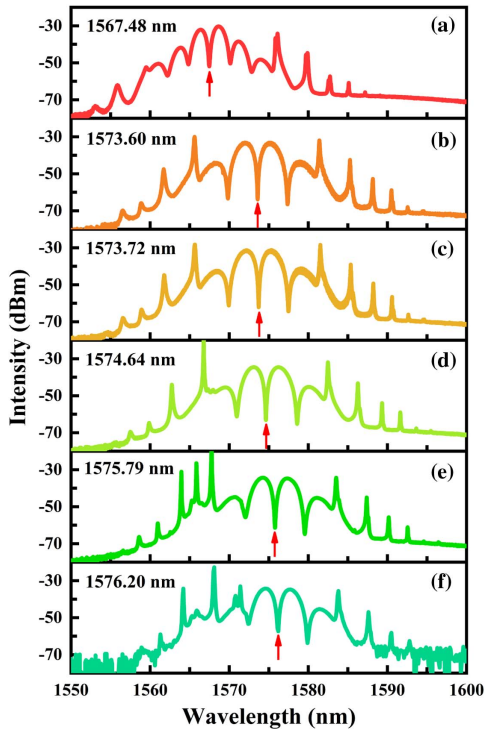


**Fig. 4.** Tunable wavelength spectra in tight soliton pairs.

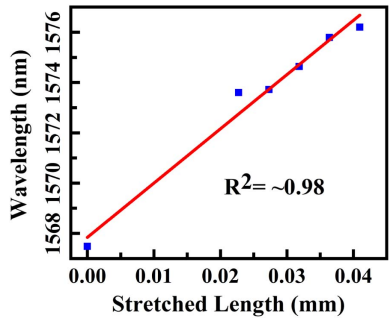


**Fig. 5.** Relationship between the stretched length of the SA and wavelength.

### D. Tunable Spatial Modulation Period and Soliton Separation of Loose Soliton Pairs

As mentioned above, the soliton property renders the conventional solitons with unique new features of interaction, which leads to formation of stable bound solitons. The bound solitons are vulnerable to the change in laser cavity parameters, e.g., dispersion, nonlinearity, gain, and loss. By properly adjusting the PC, a tuning of the loss and the intra-cavity birefringence can be achieved [32], and the transformation of different bound soliton states can be easily obtained. Thus, with further appropriate adjustment of the PC, the output pulses are transformed from tight soliton pairs to loose soliton pairs at the same pumping power of ~70 mW. Depending on the precise NCF-GIMF

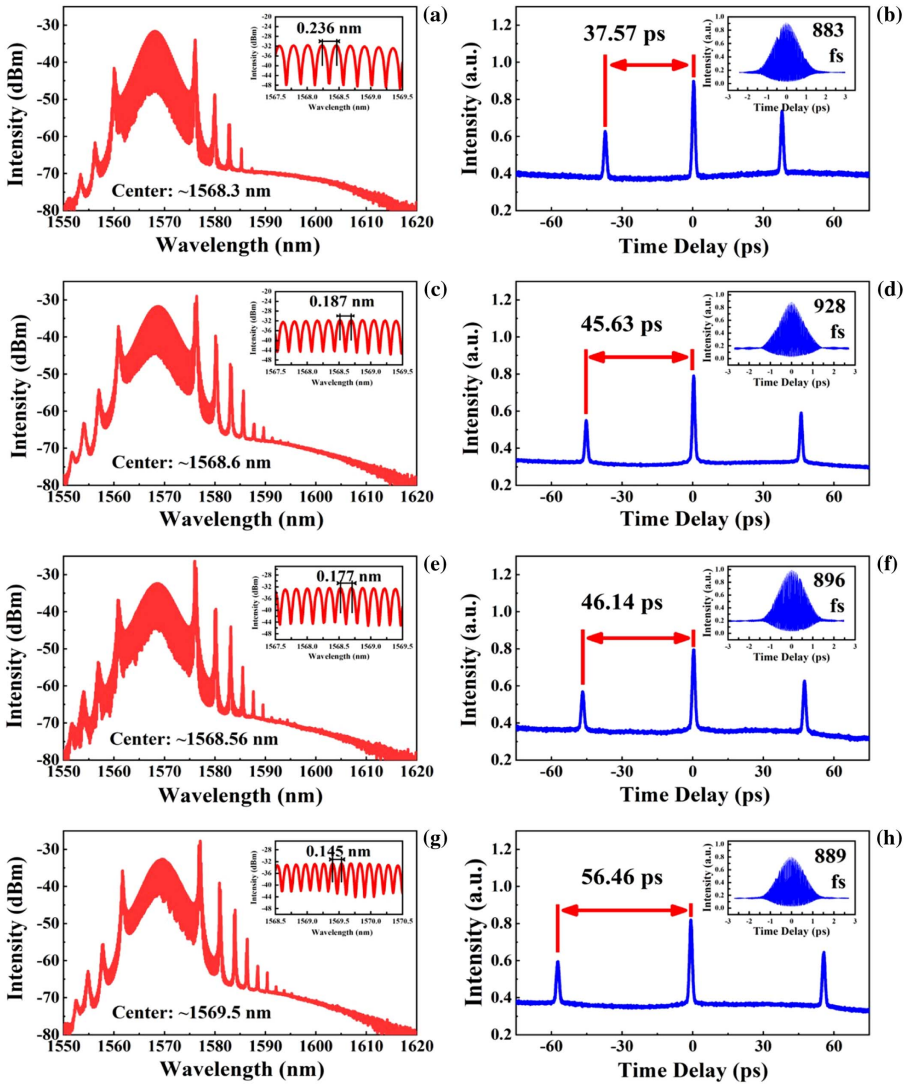


**Fig. 6.** Autocorrelation traces with different spectral modulation periods. The profiles in red are optical spectra with details in enlarged scale in the corner. The profiles in blue are autocorrelation traces with pulse width in the corner, corresponding to the panels on the left.

device conditions, the loosely bound solitons with various spectral modulation periods are realized. For example, as depicted in Fig. 6(a), an optical spectrum with stable interference fringes has a high-contrast modulation period of 0.236 nm with an amplitude of ~16 dB. The pulse separation in Fig. 6(b), measured to be ~37.57 ps, is 43 times the pulse duration of 883 fs. Thus, the state can be verified as the loosely bound solitons. The formation of the bound solitons is attributed to the balance of internal attraction and repulsion between the soliton pairs introduced by the soliton-continuum interaction process [16], which is a periodical function with a series of equilibrium points. Similarly, in our experiment, the stretching of the NCF-GIMF device results in slight perturbation on the transmission peak and modulation depth of the device; such perturbation eventually evolves into another new balance. Figures 6(a)–6(h) illustrate the characteristics of the loosely bound solitons with various pulse separations at different stretching lengths in a range of ~10 μm. The pulse separation is tuned from 37.57 ps to 56.46 ps, and the corresponding spatial modulation period shrinks from 0.236 nm to 0.145 nm. The pulse separation of these two bound states is larger than 40 times the soliton pulse durations, indicating that these pulses are all loosely bound. Moreover, the modulation amplitude decreases from 14.51 dBm to 9.29 dBm. During the tuning operation, both the pulse width and intensity ratio of autocorrelation traces retain relative stability. The slight shift in the central wavelength is consistent with the changes of tunable tight soliton pairs described in the previous section. The identical intensity of the two peaks at the central wavelength in optical spectra demonstrates the fixed $\pi$ phase difference of two pulses, as shown in the insets in Figs. 6(a), 6(c), 6(e), and 6(g).

Table 1 presents a more detailed description of the evolution of the loosely bound solitons. The intensity ratio of autocorrelation traces quickly grows with further increase of pulse separation. It can be seen in Table 1 that the pulse separation is reversely related to the spectral modulation period, which can be verified by Fourier transform, and can also be deduced from the following formula:

**Table 1. Detailed Characteristics of Loosely Bound Solitons Corresponding to Fig. 6[a]**

| F. N. | M. P. | C. W. | P. S. | I. R. | M. A. | P. W. |
|---|---|---|---|---|---|---|
| Figures 6(a) and 6(b) | 0.236 nm | 1568 nm | 37.57 ps | 1:1.84:1 | 14.51 dBm | 883 fs |
| Figures 6(c) and 6(d) | 0.187 nm | 1569 nm | 45.63 ps | 1:1.83:1 | 14.15 dBm | 928 fs |
| Figures 6(e) and 6(f) | 0.177 nm | 1569 nm | 46.14 ps | 1:1.82:1 | 12.22 dBm | 896 fs |
| Figures 6(g) and 6(h) | 0.145 nm | 1570 nm | 56.46 ps | 1:1.78:1 | 9.29 dBm | 889 fs |

[a]F. N., figure number corresponding to detailed characteristics; M. P., modulation period; C. W., central wavelength; P. S., pulse–pulse separation; I. R., intensity ratio of autocorrelation traces; M. A., modulation amplitude; P. W., pulse width.

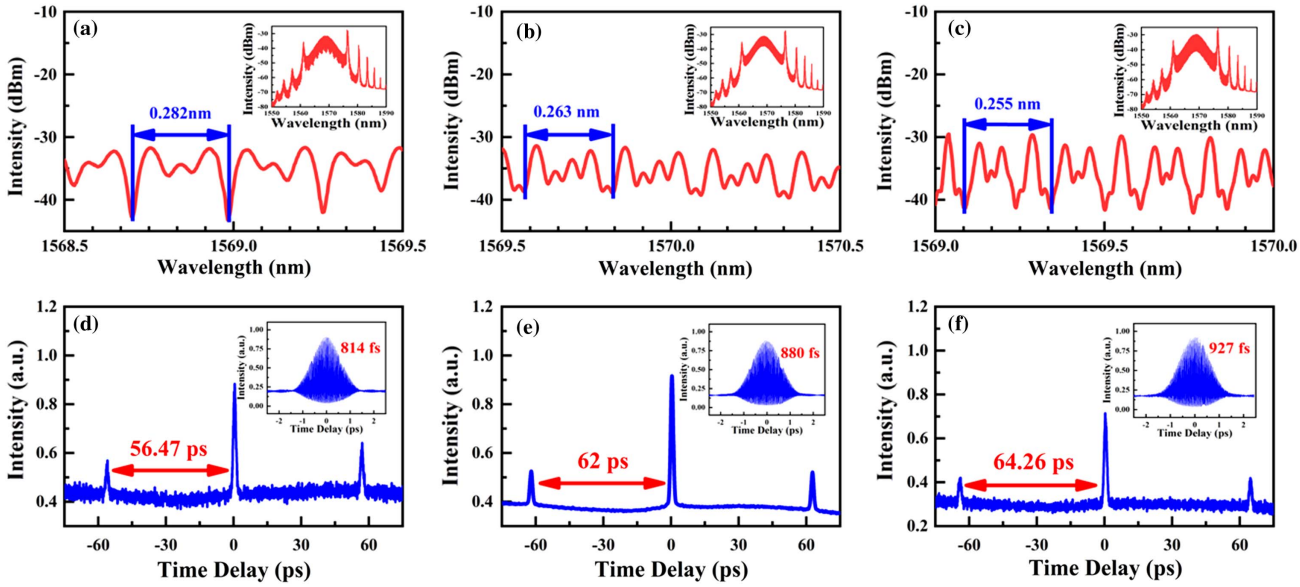


**Fig. 7.** (a)–(c) Different spectra of quasi-bound pairs; (d)–(f) corresponding autocorrelation traces.

$$\Delta\lambda = \frac{C}{\Delta\tau}, \tag{1}$$

where $\Delta\lambda$ is the absolute wavelength difference between the two peaks, and $C$ represents the light speed in vacuum. $\Delta\tau$ refers to the time separation of the two pulses. Equation (1) indicates that an inverse relation between the pulse separation and the modulation period exists.

It should also be noted that the modulation amplitude of the spectrum decreases with the increase in pulse separation. The periodic modulation waveform in the spectrum is realized by the interaction between two solitons. The relatively small separation between solitons contributes to the interaction, which directly enlarges the modulation amplitude.

During the tuning process, by appropriately adjusting the PC, we also observe some distinctive states of soliton pairs. As shown in Figs. 7(a)–7(c), the optical spectrum with a clear modulation period has a complex internal interference structure. The modulation period varies from 0.282 nm to 0.263 nm and then to 0.255 nm. The pulse separations in Figs. 7(d)–7(f), measured to be 56.47 ps, 62 ps, and 64.26 ps, respectively, are ~70 times their corresponding pulse durations of 814 fs, 880 fs, and 927 fs. This proves that the states are still loosely bound solitons, and the huge pulse separations reflect that the bound state is going to disintegrate. The three-peak autocorrelation traces have an ~1:3.5:1 intensity ratio, indicating a certain intensity difference in the two solitons. Also, the complex modulation outlines in the spectrum can be changed by slightly stretching the NCF-GIMF. As shown in Figs. 7(a)–7(c), there are in turn 3, 5, and 4 small peaks in the modulation period, which shows remarkable regularity. This phenomenon is due to the long-range soliton interactions of bound solitons [33]. With a relatively large soliton separation, the direct soliton interaction is too weak to play a role, and the long-range soliton interaction is produced when the resonant dispersive waves start working. Thus, the soliton pairs can exhibit relative oscillations. As the strength of dispersive waves in a fiber laser can be controlled only by slightly adjusting the pump power, or changing the linear cavity phase delay bias [10], the waveform in the spectrum of long-range soliton pairs can be readily in control.

## 4. CONCLUSION

In summary, we experimentally observed tightly and loosely bound soliton pairs of soliton molecules with $\pi$ phase difference of the spectrum in an Er-doped net anomalous dispersion ring fiber laser by using the NCF-GIMF structured SA. By modest stretching manipulation, we realized tunable soliton pairs from 1567.48 nm to 1576.20 nm. By slightly adjusting the PC,

loose soliton pairs can be obtained. We also have found that the two bound pulse separation is inversely proportional to both the spectral modulation period and the modulation amplitude. Also, we realized a controllable spectrum waveform of long-range bound soliton pairs. The results obtained might provide some inspiration for the study of the application of bound states in optical telecommunication systems.

## REFERENCES


1. D. Y. Tang, L. M. Zhao, B. Zhao, and A. Q. Liu, "Mechanism of multisoliton formation and soliton energy quantization in passively mode-locked fiber lasers," Phys. Rev. A **72**, 1–38 (2009).
2. M. Olivier and M. Piché, "Origin of the bound states of pulses in the stretched-pulse fiber laser," Opt. Express **17**, 405–418 (2009).
3. P. Wang, K. Zhao, L. Gui, X. Xiao, and C. Yang, "Self-organized structures of soliton molecules in 2-μm fiber laser based on $MoS_2$ saturable absorber," IEEE Photon. Technol. Lett. **30**, 1210–1213 (2018).
4. B. A. Malomed, "Bound solitons in the nonlinear Schrödinger/Ginzburg-Landau equation," in *Large Scale Structures in Nonlinear Physics*, Lecture Notes in Physics (Springer, 1991).
5. N. Akhmediev, A. Ankiewicz, and J. Soto-Crespo, "Multisoliton solutions of the complex Ginzburg-Landau equation," Phys. Rev. Lett. **79**, 4047–4051 (1997).
6. N. N. Akhmediev, A. Ankiewicz, and J. M. Soto-Crespo, "Stable soliton pairs in optical transmission lines and fiber lasers," J. Opt. Soc. Am. B **15**, 515–523 (1998).
7. D. Y. Tang, P. D. Drummond, W. S. Man, H. Y. Tam, and M. S. Demokan, "Observation of bound solitons in a passively mode-locked fiber laser," in *Quantum Electronics and Laser Science Conference* (2000), paper QWG4.
8. L. Gui, P. Wang, Y. Ding, K. Zhao, C. Bao, X. Xiao, and C. Yang, "Soliton molecules and multisoliton states in ultrafast fibre lasers: intrinsic complexes in dissipative systems," Appl. Sci. **8**, 201 (2018).
9. P. Grelu and J. M. Soto-Crespo, "Multisoliton states and pulse fragmentation in a passively mode-locked fibre laser," J. Opt. B Quantum Semiclass. Opt. **6**, S271–S278 (2004).
10. D. Y. Tang, B. Zhao, L. M. Zhao, and H. Y. Tam, "Soliton interaction in a fiber ring laser," Phys. Rev. E **72**, 1–51 (2005).
11. A. Komarov, F. Amrani, A. Dmitriev, K. Komarov, D. Meshcheriakov, and F. Sanchez, "Multiple-pulse operation and bound states of solitons in passive mode-locked fiber lasers," Int. J. Opt. **2012**, 418469 (2012).
12. A. Hideur, B. Ortaç, T. Chartier, M. Brunel, H. Leblond, and F. Sanchez, "Ultra-short bound states generation with a passively mode-locked high-power Yb-doped double-clad fiber laser," Opt. Commun. **225**, 71–78 (2003).
13. B. Ortac, A. Hideur, M. Brunel, C. Chedot, J. Limpert, A. Tunnermann, and F. O. Ilday, "Generation of parabolic bound pulses from a Yb-fiber laser," Opt. Express **14**, 6075–6083 (2006).
14. H. P. Li, H. D. Xia, Z. Jing, J. K. Liao, X. G. Tang, Y. Liu, and Y. Z. Liu, "Dark pulse generation in a dispersion-managed fiber laser," Laser Phys. **22**, 261–264 (2012).
15. W. C. Chen, Z. C. Luo, W. C. Xu, D. A. Han, and H. Cao, "Effect of gain media characteristics on the formation of soliton molecules in fiber laser," Laser Phys. **21**, 1919–1924 (2011).
16. P. Wang, X. Xiao, and C. Yang, "Quantized pulse separations of phase-locked soliton molecules in a dispersion-managed mode-locked Tm fiber laser at 2 μm," Opt. Lett. **42**, 29–32 (2017).
17. P. Wang, C. Bao, B. Fu, X. Xiao, P. Grelu, and C. Yang, "Generation of wavelength-tunable soliton molecules in a 2-μm ultrafast all-fiber laser based on nonlinear polarization evolution," Opt. Lett. **41**, 2254–2257 (2016).
18. J. Wang, M. Yao, C. Hu, A. Ping Zhang, Y. Shen, H. Tam, and P. K. A. Wai, "Optofluidic tunable mode-locked fiber laser using a long-period grating integrated microfluidic chip," Opt. Lett. **42**, 1117–1120 (2017).
19. Y. Xiang, Y. Luo, B. Liu, Z. Yan, Q. Sun, and D. Liu, "Observation of wavelength tuning and bound states in fiber lasers," Sci. Rep. **8**, 6049 (2018).
20. L. Gui and C. Yang, "Soliton molecules with $\pm\pi/2$, 0, and $\pi$ phase differences in a graphene-based mode locked erbium-doped fiber laser," IEEE Photon. J. **10**, 1502609 (2018).
21. K. Li, Y. Song, J. Tian, H. Guoyu, and R. Xu, "Analysis of bound-soliton states in a dual-wavelength mode-locked fiber laser based on Bi2Se3," IEEE Photon. J. **9**, 1400209 (2017).
22. X. Li, K. Xia, D. Wu, Q. Nie, and S. Dai, "Bound states of solitons in a fiber laser with a microfiber-based $WS_2$ saturable absorber," IEEE Photon. Technol. Lett. **29**, 2071–2074 (2017).
23. Y. Chen, S. Chen, J. Liu, Y. Gao, and W. Zhang, "Sub-300 femtosecond soliton tunable fiber laser with all-anomalous dispersion passively mode locked by black phosphorus," Opt. Express **24**, 13316–13324 (2016).
24. Z. Wang, D. N. Wang, F. Yang, L. Li, C. Zhao, B. Xu, S. Jin, S. Cao, and Z. Fang, "Er-doped mode-locked fiber laser with a hybrid structure of a step-index-graded-index multimode fiber as the saturable absorber," J. Lightwave Technol. **35**, 5280–5285 (2017).
25. Z. Wang, D. N. Wang, F. Yang, L. Li, C. Zhao, B. Xu, S. Jin, S. Cao, and Z. Fang, "Stretched graded-index multimode optical fiber as a saturable absorber for erbium-doped fiber laser mode locking," Opt. Lett. **43**, 2078–2081 (2018).
26. Z. T. Wang, Y. Chen, C. J. Zhao, H. Zhang, and S. C. Wen, "Switchable dual-wavelength synchronously *Q*-switched erbium-doped fiber laser based on graphene saturable absorber," IEEE Photon. J. **4**, 869–876 (2012).
27. P. Grelu and N. Akhmediev, "Dissipative solitons for mode-locked lasers," Nat. Photonics **6**, 84–92 (2012).
28. J. Peng, L. Zhan, S. Luo, and Q. S. Shen, "Generation of soliton molecules in a normal-dispersion fiber laser," IEEE Photon. Technol. Lett. **25**, 948–951 (2013).
29. A. Mafi, P. Hofmann, C. J. Salvin, and A. Schulzgen, "Low-loss coupling between two single-mode optical fibers with different mode-field diameters using a graded-index multimode optical fiber," Opt. Lett. **36**, 3596–3598 (2011).
30. P. Hofmann, A. Mafi, C. Jollivet, T. Tiess, N. Peyghambarian, and A. Schulzgen, "Detailed investigation of mode-field adapters utilizing multimode-interference in graded index fibers," J. Lightwave Technol. **30**, 2289–2298 (2012).
31. D. Y. Tang, L. M. Zhao, and B. Zhao, "Multipulse bound solitons with fixed pulse separations formed by direct soliton interaction," Appl. Phys. B **80**, 239–242 (2005).
32. L. M. Zhao, D. Y. Tang, X. Wu, and H. Zhang, "Dissipative soliton generation in Yb-fiber laser with an invisible intracavity bandpass filter," Opt. Lett. **35**, 2756–2758 (2010).
33. L. Socci and M. Romagnoli, "Long-range soliton interactions in periodically amplified fiber links," J. Opt. Soc. Am. B **16**, 12–17 (1999).